Chapter 9
Magnetism of Metal Phthalocyanines

Juan Bartolomé, Carlos Monton, and Ivan K. Schuller

Abstract Metal-phthalocyanine (MPc) are uniquely suited for the exploration of the intrinsic mechanisms which gives rise to molecular magnetism. In this chapter, we review the structural and magnetic properties of bulk crystal, thin film and single MPcs molecules adsorbed on different substrates. Traditional magnetic measurements and new techniques like x-ray magnetic circular dichroism show that the magnetic behavior of MPc molecules is strongly related with the electronic ground state of the central metal atom hybridized with the ligand states (intra-molecular interaction). In bulk and thin films, with stacked molecules, intermolecular exchange interactions between magnetic M atoms regulates their magnetic properties. Moreover experimental results show that the magnetic properties of single molecules are strongly affected by the electronic coupling to the supporting substrate.

9.1 Introduction

Since their discovery and later systematic studies of their molecular structure [1, 2], Phthalocyanines [3–5] have been subject of research because of their multiple applications such as dyes, catalysts and coatings. At present they are one of the most studied organic materials for possible applications in nanodevices and spintronics [6, 7]. This chapter describes the magnetic properties of Metal Phthalocyanines in bulk solid state phases, thin films and isolated molecules on various substrates. It also summarizes their recently expanding applications in molecular magnetism with a future perspective given at the end.

J. Bartolomé (✉)
Instituto de Ciencia de Materiales de Aragón and Departamento de Física de la Materia Condensada, CSIC–Universidad de Zaragoza, C/Pedro Cerbuna 12, 50009 Zaragoza, Spain
e-mail: barto@unizar.es

C. Monton · I.K. Schuller
Center for Advanced Nanoscience, Department of Physics, University of California San Diego, 9500 Gilman Drive, La Jolla, CA 92093, USA

J. Bartolomé et al. (eds.), *Molecular Magnets*, NanoScience and Technology,
DOI 10.1007/978-3-642-40609-6_9,

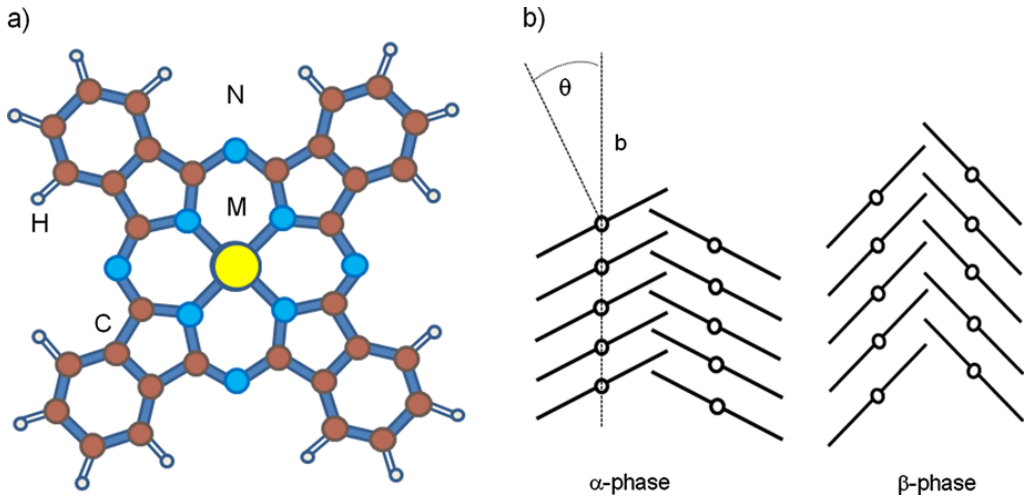

Fig. 9.1 (**a**) M-Phthalocyanine molecule. (**b**) Schematic stacking of the herring-bone α- and β-phases. θ, angle between the z axis of the molecule and the b axis of the crystal structure

9.2 Solid State MPcs

The MPc is a macrocyclic planar aromatic molecule (Pc) in which a central metal atom (M) is bound to the organic structure through four inwardly projecting nitrogen centers (Fig. 9.1(a)). Interestingly, in these molecules a large number of M substitutions are possible, giving rise to special physical and chemical properties [8]. In the present chapter only the transition metal substitutions M = Mn, Fe, Co, Ni and Cu compounds will be reviewed since they are the most relevant MPcs in the field of molecular magnetism.

Bulk MPcs crystals grow in high aspect ratio needle-shapes, a consequence of their strong anisotropic molecular structures. This anisotropy arises from the van-der-Waals molecule-molecule interactions which are greatest when the plate-like molecules are face-to-face rather than side-to-side. Such an affinity gives rise to molecule stacking in which the central metal atoms form one-dimensional (1D) chains. The stacking axis is defined by the direction of these chains, which define the b-axis, as shown in Fig. 9.1(b). In some MPcs strong intrachain and weak interchain coupling between metal atoms exist resulting in new anisotropic, optical, electrical and magnetic properties [7].

The angle between the b-axis and the normal to the plane of the molecule θ, together with the intermolecular distance, gives rise to different polymorphs, the most abundant being the α and β-phases (see Fig. 9.1(b)). The β-phase is mostly found in bulk crystals is stable and characterized by $\theta \sim 45°$. In contrast, the α-phase is metastable with $\theta \sim 25°$ angle found in bulk and often in thin films at room temperature. Table 9.1, summarizes the available structural data for solid (bulk) phase and thin film MPc molecules.

The MPc´s magnetic properties depend basically on the electronic ground state of the M substitution, which, in turn, are determined by the nearest neighbor coordination and MPc polymorphism. The molecular symmetry of MPc is very close to D_{4h} point group (see Fig. 9.1(a)), which in a simple approximation implies that the

Table 9.1 Phases and structural parameters of the MPc molecules in bulk and film phases. (θ: angle between b-axis and normal to the molecule; β: angle between ab and ac planes)

MPc	S. Group	a (Å)	b (Å)	c (Å)	θ (deg)	β (deg)	References
α'-MnPc (film)	Rhombohedral	17.60	17.60	17.6	25.0	82.0	[9]
β-MnPc	$P2_1a$	19.40	4.76	14.61	47.9	120.7	[10]
α-FePc	Monoclinic	25.50	3.77	25.2	26.5	90.0	[11]
β-FePc	$P2_1a$	19.39	4.78	14.60	47.3	120.8	[10]
α'-CoPc (film)	C2/c	25.88	3.75	24.08	26.5	90.4	[12]
β-CoPc	$P2_1c$	14.54	4.77	19.35	47.3	120.8	[13]
α'-NiPc (film)	C2/c	26.15	3.79	24.26	~26.5	94.8	[12]
β-NiPc	$P2_1a$	19.90	4.71	14.90	~46.5	121.9	[14]
α'-CuPc (film)	C2/c	25.92	3.79	23.92	26.5	90.4	[12, 15]
β-CuPc	$P2_1a$	19.60	4.79	14.60	46.5	120.6	[14, 15]

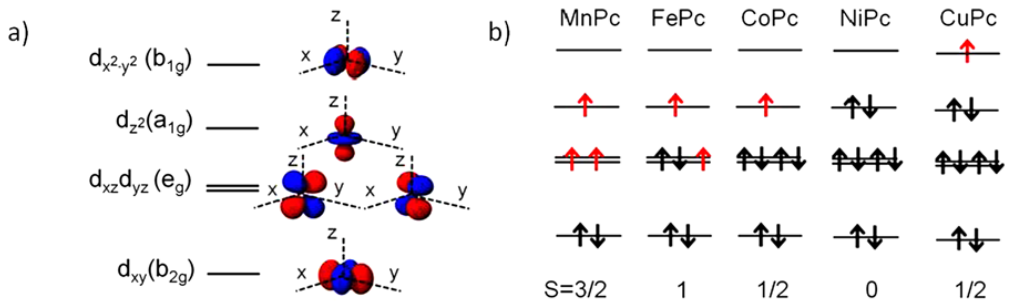

Fig. 9.2 (**a**) Metal-d orbitals with respect to the Pc molecule axes (notation as irreducible representations in D_{4h} symmetry). Spatial electron probability density of the orbitals. Blue and red identify the different complex wave function phases. (**b**) Electron filling scheme for MPc's (*black*) paired electrons and (*red*) un-paired electrons. Below, total spin due to the unpaired electrons

M d-orbitals can be classified according to a square-planar ligand-field. The mono-electronic d-states are denoted by the irreducible representation under which each transforms in the D_{4h} symmetry (and in the Cartesian coordinates notation). With this the five metal d-orbitals transform as: $a_{1g}(d_{z^2})$, $b_{1g}(d_{x^2\text{-}y^2})$, $e_g(d_{zx}, d_{yz})$ and $b_{2g}(d_{xy})$ (see Fig. 9.2(a)). The different M substitutions supply the electrons that fill consecutively these states (see Fig. 9.2(b)).

The M atom electronic states are hybridized with the phthalocyanine molecular orbitals (MO), generating the total MO, with dominant 3d electron character arising from M. The gas phase MOs for M = Mn, Fe, Co, Ni and Cu have been calculated in a series of works [16, 17] using density functional theory (DFT). These calculations incorporate hybrid states with π and σ character. The most relevant MO states to the magnetic properties are the ^3e_g, a_{1u}, a_{2u} and the $^4e_g * \pi$ antibonding states, which may hybridize with d-orbitals as seen in Fig. 9.3. The e_g MO states results from the interaction between the Fe (d_{xz}, d_{yz}) and the nitrogen (N)-p_z states of the delocalized π system. The a_{1g} MO state results from the interaction of Fe d_{z^2} states and the N-s and N-p_{xy} states, pointing toward the metal center (i.e. parallel

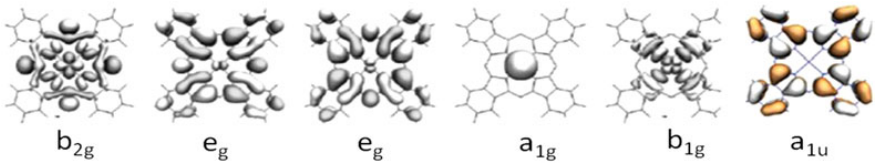

Fig. 9.3 Electron probability density of the molecular orbital states formed by the coupling of M and ligand p-states identified by the irreducible representation with respect to the D_{4h} point group [19, 20] (Reprinted Figure with permission from Betti et al. [20]. Copyright 2012 by the American Chemical Society)

to the substrate). The b_{2g} MO results from the interaction of Fe d_{xy} states and the N-p_{xy} states, orthogonal to the metal center. In the same way the b_{1g} MO state is the combination of the Fe $d_{x^2-y^2}$ states with the N-p_{xy} states pointing toward the metal center. The overlap between the metal and organic states determines the relative energy ordering of these MO states. Besides, for example, in CuPc the a_{1u} MO state is the highest occupied molecular orbital (HOMO) and the $^2e_g(\pi)$ orbital is the lowest unoccupied molecular orbital (LUMO) [18]. These MO states have wavefunctions fully localized at the macrocycles. The energy level configuration of the MO states for the transition metal substitutions was calculated for M = Fe, Co, Ni and Zn, where the LUMO and HOMO levels have been predicted showing that 3d electrons are more localized in MPc with closed shells.

Tables 9.2 and 9.3 show the experimental and theoretical information available regarding the d-electron ground states for MPcs in α and β-phases. The ground state wavefunction, made of coupled monoelectronic d-states, is described in parenthesis by the irreducible representation (irrep) under which it transforms in D_{4h} symmetry, and by the upper right index by its electron occupancy N, $(\text{irrep})^N$ (see Tables 9.2 and 9.3, 3rd column) on one hand, and as the irreducible representation of the total spin configuration in terms of the corresponding irreducible representation and its spin degeneracy n, ^{n}Xirrep (see Tables 9.2 and 9.3, 4th column), on the other hand. Some results in Table 9.3 include the ligand state occupation, as given by Ref. [18]. In many cases there are still disagreements in the reported information (i.e. β-MnPc and β-FePc ground states occupancy). Moreover, with the advent of new experimental techniques like x-ray magnetic circular dichroism (XMCD) some of these experimental conclusions are under revision.

The description of the magnetic properties of the MPc molecules is best done in terms of localized moments at the M atom. In the solid phases, there are two different crystallographic sites for the M atom. Therefore, in crystalline bulk phases, the spin Hamiltonian which describes the MPc molecules is represented by:

$$H = -2\sum_{ij} J\hat{S}_i \cdot \hat{S}_j - 2\sum_{ij} J'\hat{S}_i \cdot \hat{S}_j + \sum_j D\left(\hat{S}_j^x\right)^2 + \sum_k D\left(\hat{S}_k^y\right)^2 \tag{9.1}$$

This equation includes both, intrachain (J) and interchain (J') exchange interactions, and single-ion crystal field (D) anisotropy terms at the two different crystallographic sites (third and fourth terms).

Table 9.2 Ground state orbital occupancy determined by experimental techniques. MP refers to magnetic properties, MS magnetic susceptibility, MCD magnetic circular dichroism, XRD x-ray diffraction, XANES x-ray absorption near edge structure, XAS x-ray absorption spectroscopy, XMDC x-ray magnetic circular dichroism, PE photoemission and NMR nuclear magnetic resonance. J/k_B is the intrachain exchange. D/k_B is the crystal field parameter

MPc	Exp. technique	Ground state occupancy	Ground state	Spin	Tc (K)	J/k_B	D/k_B	Refs.
β-MnPc	MP	$(b_{2g})^2(e_g)^2(a_{1g})^1$		3/2	8.3[c]	11	28	[21]
β-MnPc	MS	$(b_{2g})^2(e_g)^2(a_{1g})^1$	$^4A_{2g}$-^4E_g	3/2	[c]			[22]
β-MnPc	MP			3/2	10[c]			[23]
α-MnPc	MP			3/2	[e]			[23]
MnPc[a]	MCD	$(e_g)^3(b_{2g})^1(a_{1g})^1$	^4E_g	3/2				[24]
MnPc[b]	XAS, PE	$(e_g)^3(b_{2g})^1(a_{1g})^1$ $(e_g)^2(b_{2g})^2(a_{1g})^1$		3/2				[25]
β-FePc	XRD	$(b_{2g})^2(e_g)^3(a_{1g})^1$	E_{gA}	1	[d]			[26]
β-FePc	MS	$(b_{2g})^2(e_g)^3(a_{1g})^1$	^3E_A	1	[d]			[27]
β-FePc	XANES	$(a_{1g})^2(e_g)^3\ (b_{2g})^1$	^3E	1	[d]			[28]
β-FePc	MS		^3B_g	1	[d]			[29]
α-FePc	MP	$(b_{2g})^2(e_g)^3(a_{1g})^1$	E_{gA}	1	5[c]	25.7 76[h]	53.2	[30]
FePc[b]	XAS, PE	$(b_{2g})^2(e_g)^3(a_{1g})^1$ $(b_{2g})^2(e_g)^2(a_{1g})^2$		1				[30]
β-CoPc	MS	$(b_{2g})^2(e_g)^4(a_{1g})^1$		1/2	[d]			[31–33]
α-CoPc	XAS, XMCD	$(e_g)^{3.8}(b_{2g})^2(a_{1g})^{1.2}$	$^2A_{1g}$-^2E_g	1/2				[34]
CoPc[b]	XAS, PE	$(e_g)^4(b_{2g})^2(a_{1g})^1$		1/2	[d]			[25]
β-CuPc	MP			1/2	[d]	0		[23]
β-CuPc	MS	$(b_{2g})^2(e_g)^4(a_{1g})^2(b_{1g})^1$		1/2	[d]			[31, 33]
β-CuPc	NMR				[g]	0.286		[35]
α-CuPc[b]	MP			1/2	[e]	~ 1.5		[23]
CuPc[b]	XAS, PE	$(b_{2g})^2(e_g)^4(a_{1g})^2(b_{1g})^1$		1/2	[d]			[25]
β-NiPc	MS	$(b_{2g})^2(e_g)^4(a_{1g})^2$		0	[f]			[31, 36]

[a] In Ar matrix, [b] thin film, [c] ferromagnetic, [d] paramagnetic, [e] antiferromagnetic, [f] diamagnetic, [g] one dimensional chain, [h] intrachain interaction (J/k_B) obtained from the soliton-kink model for $s = 1/2$

In general, most of the bulk solid state MPcs remain paramagnetic down to the lowest achievable temperatures because the molecule-molecule interaction is too weak to sustain long range order. However NiPc, β-MnPc and α-FePc are exceptions. Both polymorphs of NiPc are diamagnetic on account of their completely filled orbitals. On the contrary, β-MnPc and α-FePc polymorphs, develop long range ferromagnetism below an ordering temperature, T_c, caused by weak interchain interactions (see Tables 9.2 and 9.3). As a summary of the current understanding of the MPc's magnetic properties, we describe briefly the properties of each MPc compound.

Table 9.3 Ground state orbital occupancy obtained from theory. DFT refers to density functional theory

MPc	Theoretical method	Ground state occupancy	Ground state	Spin	References
β-MnPc	AB initio	$(b_{2g})^1(e_g)^3(a_{1g})^1$	^4E_g	3/2	[37]
MnPc$^{(im)}$	DFT		^4E_g	3/2	[38]
β-FePc	DFT		$^3B_{2g}/^3A_g$		[17]
β-FePc	DFT	$(b_{2g})^2(a_{1u})^2(a_{1g})^2(1e_g)^2$	$^3A_{2g}$	1	[18]
β-FePc	AB initio	$(b_{2g})^1(e_g)^4(a_{1g})^1/(b_{2g})^2(e_g)^3(a_{1g})^1$	$^3E_g/^3B_{2g}$	1	[37]
β-CoPc	AB initio	$(b_{2g})^2(e_g)^4(a_{1g})^1$	$^2A_{1g}$	1/2	[37]
β-CoPc	DFT	$(a_{1g})^2(a_{1u})^2(1e_g)^3$	^1E_g	1/2	[18]
CoPc$^{(im)}$	DFT		$^2A_{1g}$	1/2	[38]
β-CuPc	DFT		$^2B_{1g}$	1/2	[18]
β-NiPc	DFT		$^1A_{1g}$	0	[18]

$^{(im)}$ Isolated molecule

Mn-Phthalocyanine This compound presents both ferromagnetism (FM) and antiferromagnetism (AFM) in the β or α-phase polymorphs, respectively. In MnPc the intrachain superexchange interactions via the organic ring (Pc)π MO compete in sign. For example, the Mn-Mn FM coupling is promoted by d-electrons a_{1g}–a_{1g} interactions via the e_g filled π MO, while the AFM coupling is due to d-electrons e_g–e_g interaction via the e_g MO. In the early 70's Barraclough [22] found that in β-MnPc the intrachain FM interaction prevails with $J/k_B = 11$K for Mn(II) $S = 3/2$. Recently, Kataoka et al. [39] using XMCD confirmed the proposed FM coupling and determined that the ground state of β-MnPc is ^4E_g, where the a_{1g} is the HOMO level.

Crystal field splitting also plays an important role in the MPc's magnetic properties. In β-MnPc for example, the crystal field splits the Mn(II) $S = 3/2$ quadruplet into two doublets. This can be deduced from (9.1). Since the crystal field splitting is positive [22], $D = 20$ cm^{-1}, and the exchange field is $B_{ex} = 48$ T, below T_c the competing exchange interaction and the positive crystal electric field pull down the energy of the electronic state $S_z = -3/2$ below the $S_z = -1/2$ one, turning it into the ground state. Alternatively, the $S_z = -3/2$ ground state may be explained in terms of a negative effective crystal field, $D' < 0$, as proposed by Miyoshi et al. [33] In β-MnPc the interchain interactions are strong enough to give rise to FM ordering at $T_c = 8.3$ K (see Table 9.2). The magnetic structure of single crystals was deduced from neutron diffraction experiments by Mitra et al. [21]. They proposed that MnPc molecules order in a canted structure with an easy magnetization axis on the ac plane.

Fe-Phthalocyanine Direct M-M ferromagnetic interaction may occur when there is overlap between two orbital states in each metal atom, a half-filled and an empty orbital, or a half-filled and a full orbital [40]. In α-FePc direct exchange is dominant since the latter case is applicable, and the mechanism may be effective to

yield ferromagnetic interaction. Indeed, the orbital configuration of each Fe is E_{gA} $(b_{2g})^2(e_g)^3(a_{1g})^1$ (Table 9.2). Therefore, the $(e_g)^3$ orbital doublet of one Fe is triply occupied, thus it has a half filled orbital and a full orbital. It may overlap with the homologous in the nearest neighboring Fe since the interatomic distance is small. Since the Fe-Fe distance in α-FePc (0.38 nm) is smaller than in β-FePc (0.47 nm), direct FM exchange is most likely responsible for the FM correlations within the Fe chain with $J/k_B = 25.7$ K, for Fe(II) $S = 1$, while weak interchain interactions give rise to long range order transition at $T_C = 5$ K. In contrast, β-FePc remains paramagnetic above 2 K. The reason is that the crystal field parameter above 70 K is positive, $D/k_B = 53.2$ K, with $S = 1$, in other words the ground state corresponds to $S_z = 0$ while the excited state is $S_z = \pm 1$. Therefore, the ground state is non-magnetic, and the observed paramagnetism corresponds to the thermal population of the excited doublet [27]. In the α-phase, on the other hand, the intrachain exchange interaction is $J/k_B = 25.7$ K and it splits the upper doublet $S_z = \pm 1$ lowering the $S_z = -1$ level 44 K down in energy, close enough to match the $S_z = 0$ level. As a result, at low temperatures this system behaves as a $S = 1/2$ effective spin [30].

Since the metastable α-phase FePc is difficult to obtain in single crystal form, there are few studies of its magnetic properties. Evangelisti et al. [30], using magnetic measurement and Mössbauer spectroscopy, found FM behavior below $T = 10$ K in α-FePc. In contrast to the behavior of β-MnPc, the α-phase of FePc shows an unusual slow relaxation which resembles the one-dimensional slow relaxation process attributed to domain wall excitations along weakly coupled FM chains. These domain wall excitations (solitons) arise in an Ising system, i.e., when the single ion anisotropy is high compared to the intrachain interaction. Under these conditions the domain wall, labeled as a "kink", is just the separation by one lattice constant of spin-up and spin-down domains.

Two types of excitations are possible in Ising chains, kink-pair excitation (Fig. 9.4(a)), and single kink excitation at the end of the chain or at defects (Fig. 9.4(b)). Each excitation type presents the following energies $E_{a2} = 2J$ and $E_{a1} = J$ respectively. Filoti et al. [41] successfully explained the observed slow magnetic relaxation dynamics using the soliton-kink model. They took into account that α-FePc satisfies Ising chain conditions and that its magnetic ground state below T_c can be described with an effective $S = 1/2$ and an intrachain exchange interaction $J/k_B = 76 \pm 2$ K.

The temperature dependence of the relaxation time constant can be described by an Arrhenius law, $\tau = \tau_0 \exp(-E_a/k_B T)$, where E_a is the soliton activation energy. The temperature dependence of the frequency dependent ($10 < f < 5000$ Hz) susceptibility shows two peaks arising from a single or double kink excitations with $E_{a1} = 72$ K and $E_{a2} = 116$ K respectively, and the same $\tau_0 = 2 \times 10^{-11}$ seconds pre-factor time constant. (See Fig. 9.4(c)). The temperature dependent Mössbauer spectra show an excess electron spin flip linewidth broadening due to the propagation of the kink (or double kinks) along the chain. The flip rate Γ_ω is proportional to the product of the wall density and the average wall velocity ($n_S \times v_S$). As a consequence, the electronic spins fluctuate and the Mössbauer spectra are broadened via the hyperfine interaction with the Fe nuclei as Γ_ω approaches the Larmor

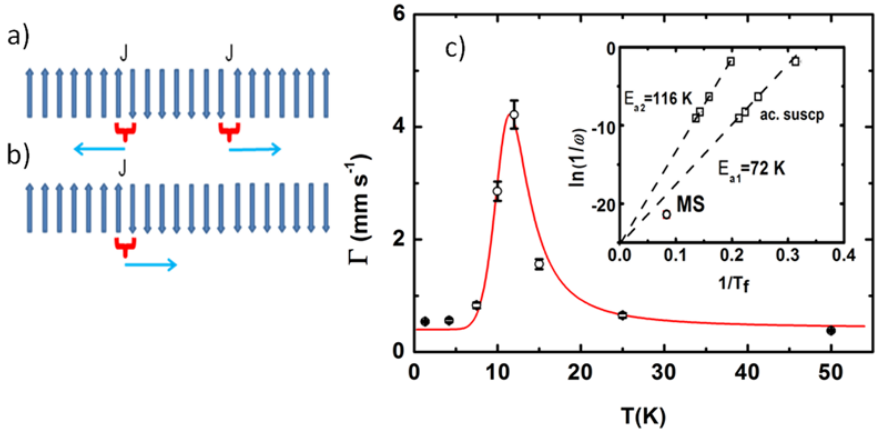

Fig. 9.4 (**a**) Double kink soliton, (**b**) single kink soliton. Keys indicate the domain wall (DW), arrows indicate the DW motion direction. (**c**) Experimental Mössbauer spectra linewidth as a function of temperature. *Dashed line* is a fit to the temperature dependence of the linewidth due to the soliton single-kink. *Inset*: Inverse of the relaxation rate, with single- and double kink soliton activation energies, as determined from a.c. susceptibility measurements (*squares*) performed at B = 800 G, and from the Mössbauer spectra [41] (*circle*)

frequency ω_L. Its temperature dependence is given by the same Arrhenius law as the ac susceptibility. The excess Mössbauer line width broadening due to solitons is given by $\Delta\Gamma \propto \Gamma_\omega/(\omega_L^2 + \Gamma_\omega^2)$ (inset of Fig. 9.4(c)). The double kink process on the other hand cannot be observed in Mössbauer spectroscopy, probably because its excitation energy falls beyond its frequency window. The spin fluctuations above T_c can also be deduced from the Single Chain Magnet model proposed in this book (Chap. 8). The relaxation processes are then described in terms of Glauber´s model for the relaxation of 1D classical chains [42]. Within this model the spin transition probability depends on the local field experienced by the spin and an Arrhenius law is predicted with an activation energy $E_a = J$ for Ising $S = 1/2$ spins, as applicable to α-FePc. Thus soliton excitation scheme explains satisfactorily the peculiar slow relaxation found below T_c in α-FePc.

Co-Phthalocyanine Both α- and β-CoPc are paramagnetic down to the lowest measured temperature. The g tensor components of both phases were determined using electron spin resonance (ESR) at 77 K of α-ZnPc and β-ZnPc diamagnetic matrices, with some Zn atoms substituted with Co(II). In both phases $g_\perp > g_{//}$, i.e. Co presents planar anisotropy. This anisotropy is more accentuated in the β-phase where the ratio $g_\perp/g_{//}$ is larger [43]. The effect of the different N adjacent positions with respect to the Co atom in the α- and β-CoPc is also detected with emission Mössbauer spectroscopy since the chemical shift and the quadrupole splitting are larger for the β-phase [44]. The anisotropic character of Co in the Pc environment is also evidenced by magnetic susceptibility. Powder β-CoPc shows a rounded maximum, characteristic of an antiferromagnetic coupled chain with $S = 1/2$. These results imply that although the intrachain interaction is rather strong ($J/k_B = -2.3$ K),

low dimensionality inhibits the establishment of long range order down to 1.8 K [33].

Cu-Phthalocyanine β-CuPc is paramagnetic down to $T = 1.7$ K, the lowest temperatures investigated so far. This paramagnetism is due to thermal fluctuation of 1D character, with a non-negligible intrachain interaction. Using NMR proton spectroscopy [35], it was determined that its spin is $S = 1/2$, and that the electron-nuclear dipolar interaction couples the proton nuclear spins of the molecule directly to the well localized electronic spins at the Cu sites. The analysis of the spin-spin relaxation time is also explained in terms of an $S = 1/2$ isotropic Heisenberg interaction with an intrachain exchange constant of $|J/k_B| = 0.286K$. An upper limit of the interchain interaction found yields a ratio $|J/J'| \geq 6.4 \times 10^3$. This limit is obtained from the lack of 1-D to 3-D crossover of the spin-lattice relaxation $T_1(\omega)$ down to the lowest measured temperature. For completeness sake, let us mention that XAS and XMCD measurements in bulk powder β-CuPc at the Cu $L_{2,3}$ edge are available [45]. The XAS features just a simple peak as expected for Cu which has an almost filled 3d orbital.

9.3 MPc Thin Films

Many different techniques, like Langmuir Blodget synthesis, spin coating [46] and organic molecular beam epitaxy (OMBE) [47] have been used to grow MPc thin films. Among these, OMBE produces MPc films with different crystalline orientation and order which depends on the substrate type. In general Cu-, Fe-, Mn-, Co- and Ni-Pc molecular planes stack parallel ("lying") to the substrate surface when deposited on Au, [48] Ag, [49–51] Cu [52]or Pd (this work), and tilted so that the MPc molecule plane is nearly perpendicular to the substrate, as has been found for FePc deposited on sapphire, [47], or on polycrystalline substrates [53] and low work function metals like Al and V [54].

Figure 9.5 shows molecular orientations in the standing and lying configurations. In spite of the molecular orientation, MPc films always grow in the lying configuration in most of metallic substrates when the temperature is kept below 200 °C during deposition. The angle θ corresponds to the stacking found in the bulk α-phase [9], however this phase is not identical since the herringbone structure is not observed. Different orientations of the adjacent MPc molecules have been reported to occur, [55, 56] therefore, we denote this structure as α'-phase. MPc films allow exploration of the anisotropic properties related to this phase.

The x ray absorption (XANES) and photoemission (PE) spectra of NiPc, CoPc and FePc thin films have been measured and a qualitative assignment of the peaks done, which show that most of the HOMO and LUMO electronic states are mainly of 3d character [58]. Angular studies using X-ray linear polarized absorption (XLPA) and X-ray magnetic circular dichroism (XMCD), at the M ion $L_{2,3}$ edges (2p $\rightarrow$ 3d electron excitations) helps relate magnetic properties to the electronic structure.

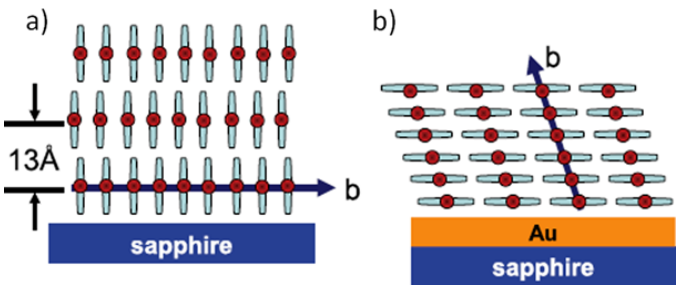

Fig. 9.5 MPc thin film stacking on a supporting surface. (**a**) Standing configuration, (**b**) lying configuration [57]

A simple analysis based on the angle dependent selection rules for the dipolar 2p → 3d excitations, has been proposed [59] to explain the XLPA and XMCD spectra. This method is based on the so-called "lighthouse-effect", namely that the absorption intensity is proportional to the number of empty valence states in the direction of the electric field of the incoming linearly polarized x-ray photons. The inset in Fig. 9.6(a) shows an incoming linearly polarized x-ray beam with the electric field contained in the incidence plane at grazing incidence. In this geometry, for MPc in the lying configuration, the electric field vector is perpendicular to the molecule plane (z axis), while for normal incidence the electric field is parallel to the molecule's xy-plane. Since the a_{1g} (d_{z^2}) orbital along the z axis has a larger density of hole states than in the xy-plane, a strong intensity variation is expected as a function of incident angle. This variation reflects the number of empty states in this specific orbital. Similar considerations can be used for the other three ligand field split 3d-states. In addition, increasing the x-ray photon energy (i.e. varying the energy of the incident x-ray beam) allows determination of the empty states above the Fermi level (see Fig. 9.6(a)). The indexing is aided by the calculated spin-split molecular orbital energy level scheme (Fig. 9.6(b)).

This analysis, first applied to a FePc α'-phase thin layer [60], implied that above the Fermi level, the 2p → 3d electron transitions to the 3d empty orbital may be indexed as follows: for increasing photon energy, to minority spin empty e_g state, with some mixing of the a_{1g} state, and to the a_{1g} state, the next excitations correspond to transitions to the e_g state in the minority antibonding states, and finally to the b_{1g} majority and minority antibonding states (see Figs. 9.6(a) and 9.6(b)).

In the following subsections the magnetic properties of different MPc compounds films are discussed.

Mn-Phthalocyanine Epitaxial thin films of MnPc were grown on a hydrogen-terminated Si [H-Si(111)] substrate. In these thin films, the molecules stack in columns up to 40 molecular layers, with the stacking axis forming an angle of $\theta = 26.5°$ with respect to the substrate plane normal, and with an intermolecular distance close to d = 3.3 Å. The angle θ corresponds to the α'-phase and becomes less definite for thicker films [9]. Such a highly textured film growth produces striking magnetic anisotropy, with the easy axis perpendicular to the substrate and antiferromagnetic intrachain interactions, in radical contrast to the ferromagnetism of bulk β-MnPc phase. This different magnetic behavior can be explained within the same model of d-electron orbitals overlap as for β-MnPc. However, the relative Mn and N

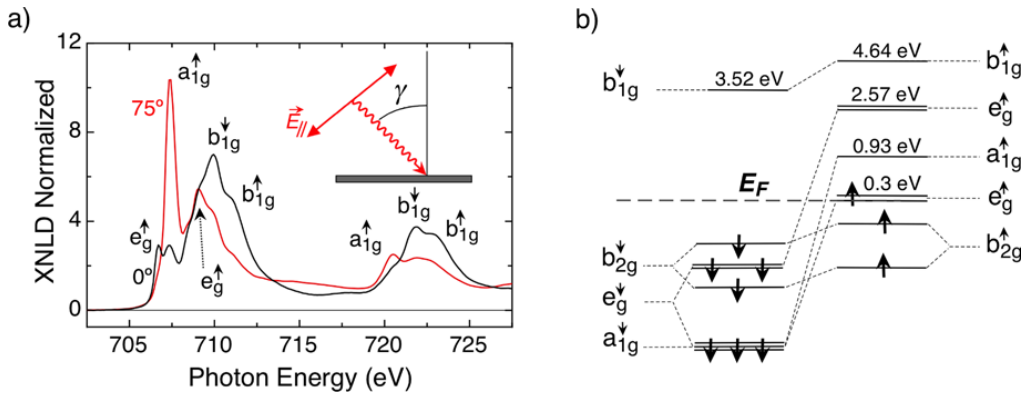

Fig. 9.6 (**a**) X-ray linear polarized absorption at the Fe L2,3 edges of FePc at different incident angles; $\gamma = 0$ (*black line*) and 75° (*red line*). The peaks are classified according to selection rules for X-ray dipolar (2p → 3d) transitions. Inset shows the incidence angle γ and the electric field vector $E_{//}$. (**b**) Spin split molecular orbital energy level scheme of FePc, where only the states with a relevant component of 3d weight ($w_{3d} > 0.05$) have been included. E_F is the Fermi energy. *Arrows* indicate the electron occupation and spin direction at each energy level [60]

positions differ between the thin film and bulk phases; the ferromagnetic exchange path via the a_g–$e_g(\pi)$ becomes weaker, while the antiferromagnetic exchange path e_g–$e_g(\pi)$, via the $e_g\pi$ MO prevails.

Fe-Phthalocyanine These films have been extensively studied since their structure and texture strongly affect their magnetic properties. The "standing" and "lying" stacking of the molecules (Fig. 9.5) can be controlled by the type of substrate as described at the beginning of this section.

In the standing case, depending on the substrate temperature during deposition, AFM and x-ray diffraction [47, 61] show that asymmetrical, elongated grains are formed. Between room temperature and 200 °C the grains consist of α'-phase FePc chains with characteristic lengths ranging from 100 to 3000 molecules, and a typical width of 25 to 80 chains [57]. When the substrate temperature is above 200 °C, the chains organize within the grain in the β-phase [62].

Below 4.5 K, the α'-phase grains order magnetically and give rise to "wasp-like" hysteresis loops. This peculiar magnetic behavior has been explained using the Preisach model with a bi-modal coercive field distribution [63] as found by optical magnetic circular dichroism (MCD) at 2 K. However, part of the hysteresis loop opening may come from slow magnetic relaxation. In contrast, the β-phase grains do not present long range order, as expected from the paramagnetism down to the lowest temperature of the bulk β-phase.

FePc film grows in the "lying" configuration on sapphire substrates covered with a 40 nm nominal thickness Au buffer layer. Annealing for one hour at 300 °C improves surface quality. For optimal crystalline growth and grain size, the substrate is kept at 150 °C during deposition [47]. The lying configuration was determined using grazing incidence XLPA at the N-K edge. The spectra corresponding to the horizontal ($\vec{E}$ field near the substrate normal) and vertical ($\vec{E}$ parallel to the substrate)

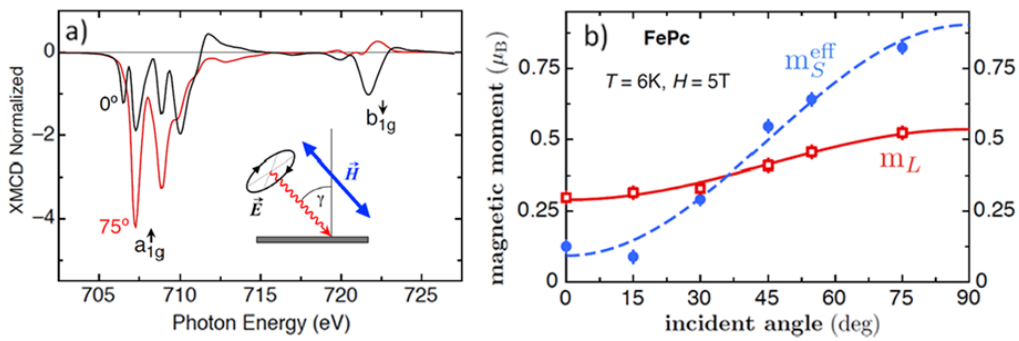

Fig. 9.7 (**a**) XMCD at the Fe $L_{2,3}$ edges of FePc, at different incident angles; $\gamma = 0$ (*black line*) and 75° (*red line*). The applied field (B = 5 T) and the helicity of the beam are parallel for every γ. (**b**) Fe spin (*blue line*) and orbital moments (*red line*) as a function of incident angle [60]

polarizations are completely different. The near disappearance of the π^* resonances for $\vec{E}$ in the molecular plane demonstrates that the four N atoms lay parallel to the substrate [60]. The molecules stack parallel to the substrate, forming chains along an axis which forms an angle of 26.5° with respect to the normal to the substrate.

The magnetization of FePc film, with the molecules parallel to the substrate, is highly anisotropic; at $T = 1.8$ K, with the magnetic field parallel to the substrate (parallel to the plane of the molecule) a magnetic hysteresis loop is observed. This loop nearly collapses when the applied field is perpendicular to the substrate plane.

The "lying" FePc film configuration has also been studied using XMCD at the Fe $L_{2,3}$ edges as a function of the incident angle. At $T = 6$ K (slightly above T_c in the paramagnetic region), a magnetic anisotropy is observed when the magnetic moments are polarized by the applied field in the parallel and perpendicular directions with respect to the substrate [60] (see Fig. 9.7(a)).

Information on the orbital and spin components of the magnetic moment of the absorbing atom projected along the field direction for a given incidence angle γ is obtained from the sum rules at the $L_{2,3}$ edges [64, 65],

$$\frac{m_L(\gamma)}{\mu_B} = -\frac{2n_h}{r}\int(\Delta\mu_{L3} + \Delta\mu_{L2})dE \tag{9.2}$$

$$\frac{m_S^{\text{eff}}(\gamma)}{\mu_B} = -\frac{3n_h}{r}\int(\Delta\mu_{L3} - 2\Delta\mu_{L2})dE \tag{9.3}$$

where $\Delta\mu_{L2,3} = \mu^-_{L2,3} - \mu^+_{L2,3}$, and $\mu^-_{L2,3}$ and $\mu^+_{L2,3}$ are the absorption measured with left (−) and right (+) circularly polarized light. The number of d holes above the Fermi energy is given by n_h.

After applying the sum rules analysis, the results are fitted to the following equations:

$$\begin{aligned} m_L &= m_L^z \cos^2\gamma + m_L^{xy}\sin^2\gamma, \\ m_S^{\text{eff}} &= m_S - 7\left(m_T^z\cos^2\gamma + m_T^{xy}\sin^2\gamma\right), \end{aligned} \tag{9.4}$$

where γ is the incident angle (Fig. 9.7(b)). The magnetic moment parameters are collected in Table 9.4. The most striking result is the easy-plane anisotropy of the orbital component of the magnetic moment, m_L^{xy} (parallel to the molecule plane), and the very large ratio with respect to the spin component, m_L/m_S. This implies that in FePc there is a highly unquenched orbital moment, with a larger component in the molecule plane. The intra-atomic dipolar term m_T is not negligible in this anisotropic FePc layered film and its contribution to the XMCD signal is associated to the planar symmetry of the ligand field.

The origin of this anisotropy is related to the orbital degeneracy of the HOMO, d-electron e_g level. In the α'-phase FePc thin layer the electronic structure can be determined from XLPA measured at the Fe $L_{2,3}$ edges as a function of incident angle, at $T = 6$ K [60]. Using the selection rules for these transitions, the spectral peaks could be indexed in terms of the spin-split molecular orbital energy level scheme [66]. Ab initio density functional calculations (DFT), including ligand field interactions, intra atomic exchange and the hybridization with the four N atoms, provide the energy levels (Fig. 9.6(b)) which explain quantitatively the measured XANES and XMCD. Comparison of these spectra to the results of the calculation suggests that an e_g orbital doublet with three electrons lies at the Fermi energy level (E_F) with the LUMO at an energy 0.3 eV above E_F and an empty state a_{1g} at 0.93 eV. The hole-hole interaction between the e_g and a_{1g} levels and the spin-orbit coupling, split the degenerate states into three doublets with a ground state with $\langle L_z \rangle = \pm\hbar$ [41]. A second order perturbation, for example, any interaction that lowers the symmetry from D_{4h} to D_{2h}, splits this doublet yielding an occupied and an unoccupied e_g level with a_{1g} mixing. The orbital moment of Fe(II) is largely unquenched, thus explaining qualitatively the large orbital moment found. The presence of the all-important e_g partially unoccupied level has been observed in electron energy-loss spectroscopy (EELS) measurements on a free-standing FePc film, in the form of a low energy excitation from the $a_{1u}(\pi)$ ligand states into the Fe (e_g) d-states [67].

The FePc electronic state has been obtained from DFT calculations of the isolated and interacting molecule cases. In the former case the ground state is found to be $^3A_{2g}$. In the latter case, the columnar stacking of the FePc molecules in α'-FePc gives the ^3E_g as the ground state because of the hybridization between MO orbitals along the b-axis. From these results one can conclude that exchange interaction has a strong effect on the electronic ground state [68].

Co-Phthalocyanine CoPc films deposited on Au(111) have been studied by XAS [69], XMCD [34] and XLPA [19]. The first two imply that the electronic ground state is a mix of $^2A_{1g}$ and ^2E_g states. However, the XLPA data analysis of the L_3 spectra indicates that the electronic ground state of CoPc is similar to that of FePc, except for the absence of the low energy e_g excitation. Since Co has one more electron than Fe, it occupies the lowest available hole located at the e_g level filling it completely. As a consequence, only one electron remains uncoupled giving rise to a total spin $S = 1/2$. For this reason, the orbital degeneracy is lost and the orbital moment may be quenched.

The XMCD at the $L_{2,3}$ edges with a $5T$ applied field as a function of incident angle, was used to determine the magnetic moment components [19] (see Table 9.4)

Table 9.4 Atomic orbital and spin component moments of M in MPcs, as determined from XMCD experiments. EDM refers to easy direction of magnetization

MPc	EDM	m_L^Z	m_L^{xy}	m_L	m_S	m_T^Z	m_L/m_S	m_T	Ref.
β-MnPc				0.21	1.45			1.66	[39]
α'-FePc	x, y	0.29(5)	0.53(4)	0.45	0.64(5)	0.074(5)	0.70(4)	1.19	[60]
α'-CoPc	x, y	0.01(3)	0.07(3)	0.05(3)	0.10(4)	0.02(3)	0.5	0.15	[19]
α'-CuPc	z	0.05(2)	0.01(1)	0.02	0.21(2)	−0.08(5)	0.1	0.23	[19]
CuPc 1 ML	z	0.20	0.045	0.096		−0.268	0.096	1.096	[45]

of a CoPc film. A strong reduction in the magnetic moment is evident, coming from a strong orbital quenching, as expected for a A_{1g} ground state. However, orbital intermixing due to spin-orbit coupling may give rise to a small contribution to the orbital moment. The easy axis magnetic anisotropy is found to be in-plane, as for FePc.

Another mechanism giving rise to small magnetic moments is the AFM intrachain coupling, already active at short range, though attenuated by thermal fluctuations. Even though this is an expected feature, as discussed in the previous section, it is noteworthy that an AFM intrachain coupling with $J/k_B = -208$ K (18 meV) has been reported using inelastic electron tunneling microscopy (IETS) [70]. We believe this is erroneous, since it differs from the reported interactions for other MPcs by 3 orders of magnitude (see Table 9.2).

Cu-Phthalocyanine In thin CuPc films there is only one strong XLPA peak at the L_3 edge that arises from the $p \rightarrow d$ electron transition to the only hole state available at the b_{1g} high energy level. XMCD shows one peak that corresponds to the excitation of a 2p electron to that hole. The analysis, in terms of the sum rules, indicates an out-of-plane easy magnetic anisotropy axis. In addition, the orbital component of the magnetic moment is very small and the spin component corresponds to $S = 1/2$. Since the orbital moment is nearly quenched for the b_{1g} state, the strong uniaxial anisotropy originates in the dipolar intra-atomic term m_T of the effective spin moment and it reflects the planar b_{1g} orbital which governs the magnetic properties of this compound [19].

9.4 MPc Molecules Adsorbed on Substrates

The very robust adsorption of MPc molecules on a wide variety of substrates, has allowed to perform non-destructive x-ray absorption experiments. Low temperature Scanning Probe Microscopy allows inducing modifications at the single molecule level. The possibility of manipulating, modifying, relocating, and constructing structures at the atomic level has been essential to develop understanding of the interaction mechanisms at the molecule-substrate interface.

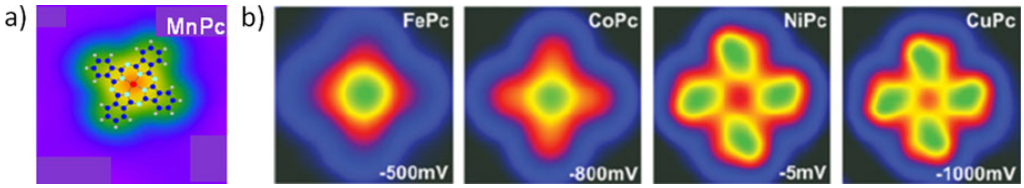

Fig. 9.8 STM topographic images of MPcs. (**a**) Image of MnPc deposited on Pb [71] (Reprinted Figure (**a**) with permission from Fu et al. [71]. Copyright 2007 by the American Physical Society). The MnPc molecular structure is superimposed. (**b**) Bias voltage dependent images of the M = Fe, Co, Ni and Cu Pcs deposited on Au(100). Note the chiral contrast for the Ni and Cu cases [51] (Reprinted Figure (**b**) with permission from Mugurza et al. [51]. Copyright 2012 by the American Physical Society)

MPcs have attracted much attention because of their self-assembling capacity on substrates [72]. For a metal substrate, hybridization of the $3d_{z^2}$ states of the metal (M) center in the MPc and the electronic states of the substrate forces the position of M on the substrate, while the orientation of the molecule is mostly influenced by the interaction of the N atoms and the surface. The relative orientation of the molecules is driven by intermolecular forces. It is now clear that the substrate on which the molecule is adsorbed plays a fundamental role in defining its magnetic state. The final state of the molecule depends on whether the substrate is a ferromagnet, a metal or a semiconductor.

Typically, a single MPc molecule adsorbed on a metallic surface appears in STM as a four-leaf clover shape with a protuberant (Fe, Co) or depressed (Cu, Ni) spot at its center (see Fig. 9.8). The MOs of the π conjugated macrocycles interact with the conducting substrate and modify the total spin of the molecule. The mechanism underlying these phenomena is known as the Kondo effect [73]. This effect is produced by resonant scattering coming from the hybridization of the magnetic impurity, in this particular case the MPc molecule, with a continuum of electronic states, in the conducting substrate. As a result, the net effect is the generation of a collective non-magnetic singlet state. The Kondo effect occurs below a characteristic temperature T_K, which defines the boundary between resonant and non-resonant behavior. When molecules assemble in clusters, the intermolecular interactions may compete with the Kondo effect and the molecules may become magnetic. The first report on Kondo screening of MPcs was done by Gao et al. [74] on FePc. In a short period after his report many researchers have dealt with this subject. Below we review some of the most prominent results on the magnetism of adsorbed MPcs on different substrates.

Mn-Phthalocyanine Single MnPc molecules were deposited by sublimation on top of Pb(111) nanoislands [71]. The molecule image consists of a four lobe cross with a protrusion at its center. The thickness of the Pb nanoisland affects strongly the Kondo resonance, with T_K oscillating as a function of the number of Pb monolayers. This feature originates in the strong confinement of the Pb electrons in films thickness ranging from 2 ML to 22 ML. By comparing STM spectra to simulations, it was concluded that the magnetic moment on Mn decreases from $3\mu_B$, for an isolated molecule, to $0.99\mu_B$ when adsorbed on Pb. The contribution to the magnetic

Table 9.5 Kondo temperature , T_K, and calculated magnetic moment, m, located at the metal atom in M-Phthalocyanine molecules adsorbed on a single-crystal substrate

Sample	Substrate	T_K (K)	$m(\mu_B)$	Reference
MnPc	Pb(111)	23–419	0.99	[71]
FePc	Au(111)	2.6 ± 1.4		[75]
Dehydrogenated CoPc	Au(111)	208	1.03	[76]
CuPc	Ag(100)	27 ± 2		[51]

moment arising from the d_{xy} orbital survives since it is less hybridized with the substrate energy bands.

Fe-Phthalocyanine Single FePc molecules which lay parallel on Au(111) single crystal surface show up as a four-leaf clover, with the organic lobes as the leafs. The clover is oriented in two configurations, at 15° with respect to each other. A bright spot protrusion, at the molecule center, is related to the d-orbital character near the Fermi surface [74]. This feature is related to the strong coupling of the a_{1g} and e_g (perpendicular) orbitals near the Fermi level with the tip states [77]. The STM spectra at the single molecule center position shows a Fano-type resonance characteristic of the Kondo effect. From its temperature dependence, the Kondo temperature T_K of the molecule and substrate collective singlet state can be determined [75] (see Table 9.5). As the density of molecules increases on the substrate, molecules self-assemble in planar clusters, forming a 2D Kondo superlattice on the metal surface. The STS spectra at the borders of these superlattices has a Fano resonance similar to that of a single molecule, however, below T_K the Fano resonance intensity at the center of the cluster is reduced and is split into two peaks. This feature is caused by the oscillatory Ruddermann-Kittel-Kasuya-Yosida (RKKY) interaction, via the conduction electrons, which generates an antiferromagnetic coupling and consequently, AFM correlations between the spins [75].

In contrast, no Kondo effect is detected when a single FePc molecule is deposited on Ag(100). This is caused by a stronger interaction of the a_{1g} and e_g perpendicular states with the substrate [51]. Basically due to the interaction between the FePc molecules and Ag, one electron is transferred from the substrate. The MPc states ^2e_g and e_g are mixed due to hybridization with the substrate while a_{1g} is the MO with the highest degree of hybridization. This modifies the charge distribution in the molecule, which consequently reduces the Fe spin value.

These results are in agreement with XMCD performed on a 1ML FePc on Au(111) [19, 34], which shows a reduced (but not completely quenched) Fe magnetic moment (Fig. 9.9). This conclusion arises from the charge transfer between the d^6 Fe configuration and the metal substrate through the d_{z^2} orbital, assuming a weak mixing with the d^7 configuration. Under this assumption, the net result is that the spin of the bound electron from the substrate couples AFM to the two lowest states of Fe, and as a consequence yields a total spin $S = 1/2$.

The conductivity of the substrate also plays an important role in the magnetic state of the adsorbed molecule. In a single FePc molecule deposited on a clean,

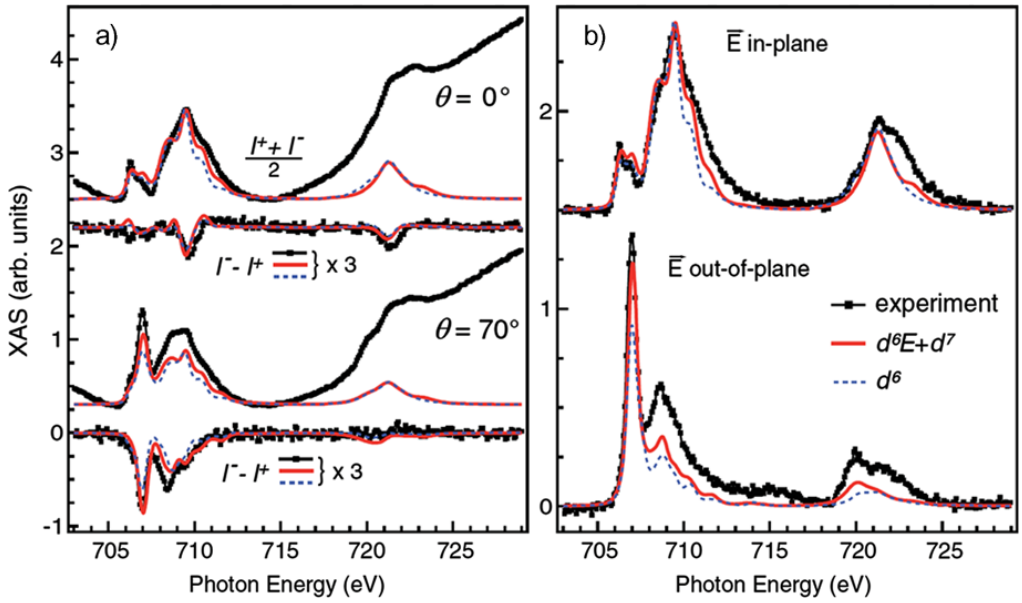

Fig. 9.9 (**a**) Circular polarized XAS (*upper*) and XMCD (*lower*) at the Fe $L_{2,3}$ edges on a 1ML FePc on Au(111) at two different incident angles θ (*black lines*). (**b**) X-ray linear polarized absorption in two polarizations. The x-ray electric field vector is either fully in-plane or out-of-plane at an angle of 20° with respect to the surface normal (*red lines*) simulations [34] (Reprinted Figure with permission from Stepanow et al. [34]. Copyright 2011 by the American Physical Society)

metallic Cu(110) substrate, the Fe magnetic state changes from the bulk S = 1 to S = 0. In contrast, when deposited on semiconducting, oxidized, Cu surface (Cu(110)(2 × 1)-O), the S = 1 state is retained, although with a different ligand field splitting than in the bulk [78].

A recent interesting development is the deposition of FePc on graphene, supported by Ir(111). FePc sub-monolayers lay flat on graphene with a 8 ± 10° angular tilt with respect to the graphene surface. Thicker deposition leads to less ordered island formation [79]. XMCD measurements, at the Fe $L_{2,3}$ edge, show clear anisotropic dichroism, indicating that magnetic properties of FePc are affected by the interaction with graphene. An increase in the planar anisotropy (more intensity due to the in-plane orbitals) with respect to α'-FePc in the thin film case (Sect. 9.3. and Table 9.4) is observed. On the other hand, the total moment of the Fe atom decreases. Both the moment and anisotropy decrease with increasing thickness [80].

Co-Phthalocyanine As for FePc deposited on Ag, STM of CoPc shows a protusion at the CoPc molecule center [51]. However, in CoPc deposited on Au(111) or Ag(100) there is no Kondo effect [51, 76]. In fact, XMCD of 1 ML CoPc shows that valence fluctuations quench the Co moment [34]. Charge transfer between the molecule and the substrate accounts for the absence of magnetic moment. This occurs because a Co excited level is occupied by an extra substrate electron which intermixes with the ground state. As a result there is a reduced a_{1g} level occupation, and the total coupled state is a non-magnetic singlet state [51]; i.e. with S = 0. In CoPc deposited on Cu(111), the N 1s XAS spectra imply that an electronic charge

redistribution, compatible with charge transfer from the substrate to the molecule, takes place upon adsorption [52].

Single CoPc molecules couple FM to Co nanoislands as shown by spin polarized STM. The magnetization density observed in this case reaches a maximum close to the Co atoms, although there is some oppositely oriented magnetic moment at the N and C atoms. The compensation of these moments leads to the quenching of the total moment [81]. Moreover, when 1ML CoPc is deposited on a metallic Fe FM film, a small but distinguishable XMCD component is detected, which indicates the presence of a non-zero moment parallel to the Fe substrate magnetization [52]. In fact, no XMCD signal is observed on a 1ML of CoPc deposited on Au(110) [19]. When the thickness increases to 6 ML this XMCD component completely disappears, as in the thick film case. In fact, no XMCD signal is observed on a 1ML of CoPc deposited on Au(110) [19]. This result is compatible with DFT calculations of the electronic structure and van der Waals (vdW) forces to determine the total molecule spin state. Although the electron supplied by the substrate fills the d_{z^2} MO state, the distortions produced by the vdW forces give rise to a spin redistribution so that spin splitting is recovered due to the molecule-surface bonding at the ligand portions of the molecule [52, 82].

A very interesting development in the field of MPcs adsorbed on metallic substrates is the possibility of manipulating the Pc ligands in order to modify the magnetic state of the molecule/substrate magnetic state. Pioneering work has shown that an STM tip may induce dehydrogenation of a single CoPc adsorbed on Au(111) [76]. The as-deposited CoPc molecule shows no Kondo effect, while in the dehydrogenated molecule there is an onset of Kondo effect, with $T_K \approx 208$ K. The STM tip removes the external H atoms of the CoPc molecule and as a consequence, favors chemical binding with the substrate via the ligands. The molecule deforms from a flat shape, prior to dehydrogenation, into a four-legged concave cap-like table with the concavity towards the surface, after H removal (Fig. 9.10(a)). The magnetic state of CoPc transforms from initially non-magnetic, to magnetic in the H-trimmed bound molecule, with a moment of $1.09\mu_B$. Curiously, such a moment is larger than that of a single Co atom directly bound to a Au atom on the Au(111) substrate. The coupling of the Co atom in the molecule with the substrate, via the H-trimmed Phthalocyanine molecule ligands, is stronger than in the direct Co-Au coupling case [76, 83].

Cu-Phthalocyanine Adsorption of sub-monolayers CuPc on Au(111), Ag(111) and Cu(111) studied with low-energy electron diffraction [84], show various degrees of binding. The binding is weak on Au (physisorption), where no charge transfer is observed. On Ag it is more intense (weak chemisorption), with charge transfer that gives rise to intermolecular repulsion. When deposited on Cu the interaction with the substrate is the strongest (strong chemisorption), and the intermolecular interaction is attractive. The symmetry reduction from fourfold to twofold caused by the different filling of the LUMO state induces an electrostatic quadrupole moment that, in turn, generates an attractive intermolecular force. These attractive forces prevail over the repulsive ones and there is a net effective attractive interaction.

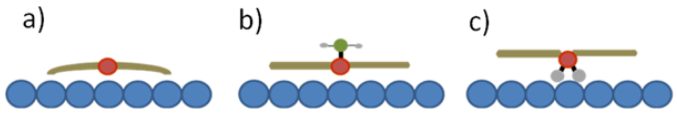

Fig. 9.10 Schematic diagram of MPc molecule deposited on a substrate (*blue circles* represent the substrate's atoms): (**a**) dehydrogenated CoPc on Au [76]. (**b**) NH_3/FePc/Au. Note the NH_3 is located in the external side of the FePc molecule [85]. (**c**) FePc/(η^2-O_2)/Ag. Note the O_2 group sandwiched between the FePc molecule and the substrate [86]

STM of CuPc adsorbed on Ag shows a depression at its center. The spin state of Cu is $S = 1/2$ and an elastic Kondo resonance is also observed. This Kondo resonance arises from the presence of an unpaired spin located at the macrocycle $^2e_g(\pi)$ orbital. The $S = 1/2$ spin couples with the Cu $S = 1/2$ to generate a $S = 1$ triplet ground state and an excited $S = 0$ singlet. This is confirmed by the presence of a strong Kondo peak at zero bias with $T_K = 27$ K.

These results may be compared to XMCD performed at the Cu $L_{2,3}$ edge on a 1ML thin film on Au, recalling that this technique is only sensitive to the Cu empty d-states. The XMCD measurements on a CuPc 1ML [19, 45] show that about 10 % of the magnetic moment is of orbital origin, and the anisotropy is perpendicular to the molecule plane. Moreover, the value of the magnetic moments is strongly enhanced with respect to that of the Cu in a thin film [19] (see Table 9.4). The anisotropic dipolar term, represented by m_T (Table 9.4) is negative in the CuPc, reflecting the uniaxial anisotropy instead of the planar one observed in FePc and CoPc.

9.5 Perspectives of MPcs

In this Section we mention briefly the research lines on MPcs that have been opened and are gaining impetus in the advancing field towards single molecule magnetic switching. This relates to the possibility of controlling the magnetic state of a molecule by external means and on single molecule spintronics.

Since the seminal work on chemical switching of magnetic properties of molecules deposited on a substrate [67], a renewed activity in the molecule state control has erupted. A planar Fe-TPA_4 (TPA = terephthalate) molecule deposited on Cu can switch the Fe in-plane magnetic anisotropy to out-of-plane when the molecule adsorbs selectively two oxygen atoms (O_2-FeTPA4) [87]. FePc deposited on a metallic substrate, and subject to adsorption of different molecules, has been used in this context also. After deposition on Au, as described in the previous section, FePc is allowed to react with different ligands. In NH_3/FePc/Au there is a weak chemisorption bonding of NH_3 with the Fe atom on the external side of the deposited FePc molecule on Au (Fig. 9.10(b)). This modifies the Fe coordination with a consequent reorganization of the Fe charge, which leads to pairing of electrons and quenching of the spin ($S = 0$). In addition, there is a weakening in the FePc-Au bonding. These conclusions are obtained from the interpretation of XPS

measurements at the $2p_{3/2}$ line combined with DFT calculations [85]. For Pyridine/FePc/Au the effect on the molecule-surface bonding and spin quenching is similar. However, in the case of NO/FePc/Au the spin quenching seems to be partial ($S = 1/2$). The mechanism causing the weakening of the FePc- substrate interaction is the capture of the gas molecule on the external side of the adsorbed molecule [88] that causes a redistribution of charges and, in turn, the dehybridization of the Fe d_{z^2} orbitals and the substrate Au(111) states.

The self-assembly of functionalized MPc's on a oxygen-reconstructed Co substrate has been used to create a checkerboard lattice of Mn(III)Pc and fluorinated Fe(II)F_{16}Pc [89]. XMCD, shows that both Fe and Mn are AF coupled to the Co substrate magnetization. In a subsequent step, dosing with NH_3 modifies the electronic state of the 3d metals; it quenches the magnetic moment of Fe ($S = 0$), while it maintains the Mn moment AF coupled to the substrate. The original state is recovered by annealing at 300 K; the Mn moment is ON (AF coupled to Co, while the Fe moment switches from ON ($S = 1/2$, AF coupled to Co) to OFF ($S = 0$). The process can be reversible, thus it allows cyclic switching. This recent achievement corroborates the very active research on the magnetic switching by external chemical activation.

The exposure to oxygen of 1 ML FePc on Ag(110) produces different binding. The most stable configuration, compatible with experimental STM and spectroscopic evidence (XAS, XPS), is the FePc/(η^2-O_2)/Ag one, where η^2-O_2 describes that each of the O atoms is bound to Fe by an Fe-O bond. In this configuration the oxygen is chemisorbed in the interfacial structure between the organic molecule and the Ag support, with the Fe of the Pc molecule placed on top of an Ag atom and the two oxygen Fe-O bonds directed towards two lateral substrate Ag atoms; i.e. the oxygen is encaged between the FePc and the Ag substrate (Fig. 9.10(c)). The effect of this configuration on the magnetic properties remains to be studied. Interestingly, the FePc/Ag system acts as a cyclic catalyst in the oxygen reduction reaction, a property that is of great interest as a substitute for Pt catalyst [86]. This implies an expanding basic and applied surface chemistry and physics activity related to molecular switching mechanisms produced by adsorption of atoms and ligands.

The possibility of creating single molecule spintronic devices, such as spin valves or spin-filters, in electrode/MPc/electrode sandwiches has been theoretically and experimentally explored recently. Particularly intriguing is the predictions that a MnPc molecule sandwiched between two semi-infinite armchair single walled carbon nanotubes may be a robust, 100 % efficient spin-filter with very high transmission around the Fermi energy [90]. The delocalization of the π type HOMO MnPc molecule states and their "pinning" with the conducting states of the carbon electrodes lead to the formation of efficient conducting channels. The same efficient spin-filter configuration is predicted to occur with the FePc molecule [91].

In addition, giant magnetoresistance (GMR) has been reported to occur through a single H_2Pc molecule. This was claimed for a molecule on a Co metal island deposited on Cu(111) surface FM electrode, with a Co coated tip as the second FM electrode. GMR as high as 60 % was measured. This was proposed to be due to the LUMO molecular states coupling to highly polarized spin minority states of Co

[92]. GMR was also found for a H_2Pc molecule sandwiched between AFM Mn as one electrode and an Fe coated ferromagnetic tip [6]. Thus, the fabrication of a single molecule phthalocyanine spin-valve may not be too far.

In the introduction of this chapter we set out to cover the magnetic properties of transition metal MPcs. However, M substitution is much richer and goes beyond the simple MPcs described above. Of particular interest to this book is the recent work on double decker phthalocyanines ($LnPc_2$), where Ln is a rare earth. In this type of molecule, the Ln(III) atom is sandwiched between two Pc molecules, rotated by 45° with respect to each other. The Ln = Tb and Dy compounds hysteresis cycle exhibits slow relaxation, similar to that of Single Molecule Magnets (SMM) formed by clusters. Interestingly, in this case however a single magnetic atom is responsible for the phenomenon, which has been therefore denoted as a "single ion magnet" (SIM) [93, 94]. The low temperature hysteresis curves show steps at certain fixed fields, similar to those in SMMs discussed in other Chapters, which have been explained as due to the existence of Magnetic Quantum Tunneling (MQT). In the very low temperature hysteresis loop in a single crystal, these occur in $TbPc_2$, less clearly in $DyPc_2$ [95], and later in $HoPc_2$ [96]. To explain the regularly spaced steps in applied magnetic field in the Ho case, and irregularly in the Tb case, a different mechanism is necessary. The steps due to magnetic tunneling resonance in SMM clusters (see Chaps. 1 and 2), take place when the field split electronic spin levels cross. In the $LnPc_2$'s this type of crossing yields to very high crossing fields compared to those observed. In fact, the non-zero nuclear spin of the Ln lends a new magnetic degree of freedom. The interactions acting on the 4f electronic ground state are the ligand field which splits the Ln free electronic states. This gives rise to a highly uniaxial anisotropic electronic spin ground state, the hyperfine interaction coupling it with the nuclear spin I and the nuclear quadrupole interaction term. Then, the steps in the $LnPc_2$ low temperature hysteresis curves occur at those applied fields for which the total energy levels (i.e. the entangled electronic J and nuclear spin states I), $\phi = |J_z\rangle|I_z\rangle$, become degenerate. Moreover, the hyperfine and the quadrupolar interactions provide the off-diagonal terms in the Hamiltonian to allow resonant tunneling at the so called, "avoided crossing" of levels, which produce the fast relaxation channels at the crossing field. The nuclear spin states degree of freedom play a crucial role for the Quantum Tunneling of $LnPc_2$ but not for the transition metal SMMs [95, 96].

Because of the chemical stability of the MPc adsorbed on different substrates and of the magnetic bi-stability, $TbPc_2$ is a natural candidate as a possible single molecule memory or quantum computing element. $TbPc_2$ has been deposited on polycrystalline Au [97] and Cu(100) substrate covered by ferromagnetic Ni thin capping layer [98]. Molecules are in the "lying" configuration i.e. with the easy magnetization axis perpendicular to the substrate. The ferromagnetic Ni layer couples antiferromagnetically with the Tb magnetic moment and stabilizes its polarization up to room temperature. In contrast to the ferromagnetic coupling present in the transition metal ferromagnetic substrate, discussed in the previous section, in $TbPc_2$ there is an intermediate Pc molecule between the Tb ion and the substrate. As a consequence, direct interaction between Tb and Ni substrate weakens and allows for the AFM superexchange coupling to prevail.

The element selectivity of XMCD has been exploited very nicely in proving the AFM character of this interaction [98]. As a function of applied field, the XMCD at the Ni L_3 and the Tb M_5 edges were measured at fixed photon energy at the XMCD peak. The field applied perpendicular to the substrate overcomes the competing AFM Tb-Ni exchange field until the Tb moment rotates and becomes aligned with the field. This first exciting result opens the possibility of using these molecules as spintronic elements at room temperature, and that new molecules and configurations can be expected to appear in the near future.

Acknowledgements J. Bartolomé acknowledges financial support from the projects MINECO (MAT2011/23791) and DGA IMANA E34. C. Monton and I.K. Schuller acknowledge the financial support of AFOSR FA9550-10-1-0409. The magnetism aspects of this work were supported by the Office of Basic Energy Science, US Department of Energy, under Grant No. DEFG03-87ER-45332. Illuminating discussions with F. Bartolomé and G. Filoti are acknowledged.

References

1. R.P. Linstead, J. Chem. Soc. **1016** (1934). doi:10.1039/jr9340001016
2. R.P. Linstead, A.R. Lowe, J. Chem. Soc. **1022** (1934). doi:10.1039/jr934000122
3. A. Braun, J. Tcherniac, Ber. Dtsch. Chem. Ges. **40**, 2709 (1907)
4. H. de Diesbach, E. von der Weid, Helv. Chim. Acta **10**, 886 (1927)
5. A.G. Dandridge, H.A. Drescher, J. Thomas, Br. Pat. Abstr. **322**, 169 (1929)
6. W. Wulfhekel, T. Miyamachi, S. Schmaus, T.K. Yamada, A.F. Takacs, A. Bagrets, F. Evers, T. Balashov, M. Gruber, V. Davesne, M. Bowen, E. Beaurepaire, in *Spintronics with Single Molecules: 12th IEEE International Conference on Nanotechnology (IEEE-NANO)*, Birmingham, UK (2012)
7. M. Evangelisti, in *Encyclopedia of Supramolecular Chemistry*, ed. by J.L. Atwood, J. Steed (Dekker, New York, 2004), p. 1069
8. M.K. Engel, *The Porphyrin Handbook* (Academic Press, New York, 2003), p. 1
9. H. Yamada, T. Shimada, A. Koma, J. Chem. Phys. **108**, 10256 (1998)
10. J.F. Kirner, W. Dow, W.R. Scheidt, Inorg. Chem. **15**, 1685 (1976)
11. C. Ercolani, C. Neri, J. Chem. Soc. A **1715** (1967). doi:10.1039/j19670001715
12. M. Ashida, N. Uyeda, E. Suito, Bull. Chem. Soc. Jpn. **39**, 2616 (1966)
13. R. Mason, G.A. Williams, P.E. Fielding, J. Chem. Soc., Dalton Trans. **676** (1979). doi:10.1039/dt9790000676
14. J.M. Robertson, J. Chem. Soc. **615** (1935). doi:10.1039/jr9350000615
15. B. Honigman, H.U. Lenne, R. Schrodel, Z. Kristallogr. **122**, 185 (1965)
16. N. Marom, L. Kronik, Appl. Phys. A, Mater. Sci. Process. **95**, 159 (2009)
17. N. Marom, L. Kronik, Appl. Phys. A, Mater. Sci. Process. **95**, 165 (2009)
18. M.S. Liao, S. Scheiner, J. Chem. Phys. **114**, 9780 (2001)
19. P. Gargiani, G. Rossi, R. Biagi, V. Corradini, M. Pedio, S. Fortuna, A. Calzolari, S. Fabris, J.C. Cezar, N.B. Brookes, M.G. Betti, Phys. Rev. B **87**, 165407 (2013)
20. M.G. Betti, P. Gargiani, C. Mariani, S. Turchini, N. Zema, S. Fortuna, A. Calzolari, S. Fabris, J. Phys. Chem. C **116**, 8657 (2012)
21. S. Mitra, A.K. Gregson, W.E. Hatfield, R.R. Weller, Inorg. Chem. **22**, 1729 (1983)
22. C.G. Barraclough, R.L. Martin, S. Mitra, R.C. Sherwood, J. Chem. Phys. **53**, 1638 (1970)
23. S. Heutz, C. Mitra, W. Wu, A.J. Fisher, A. Kerridge, M. Stoneham, T.H. Harker, J. Gardener, H.H. Tseng, T.S. Jones, C. Renner, G. Aeppli, Adv. Mater. **19**, 3618 (2007)
24. B.E. Williamson, T.C. Vancott, M.E. Boyle, G.C. Misener, M.J. Stillman, P.N. Schatz, J. Am. Chem. Soc. **114**, 2412 (1992)

25. T. Kroll, R. Kraus, R. Schonfelder, V.Y. Aristov, O.V. Molodtsova, P. Hoffmann, M. Knupfer, J. Chem. Phys. **137**, 054306 (2012)
26. P. Coppens, L. Li, N.J. Zhu, J. Am. Chem. Soc. **105**, 6173 (1983)
27. B.W. Dale, R.J.P. Williams, C.E. Johnson, T.L. Thorp, J. Chem. Phys. **49**, 3441 (1968)
28. P.S. Miedema, S. Stepanow, P. Gambardella, F.M.F. de Groot, J. Phys. Conf. Ser. **190**, 012143 (2009)
29. C.G. Barraclough, R.L. Martin, S. Mitra, R.C. Sherwood, J. Chem. Phys. **53**, 1643 (1970)
30. M. Evangelisti, J. Bartolome, L.J. de Jongh, G. Filoti, Phys. Rev. B **66**, 144410 (2002)
31. N. Ishikawa, Struct. Bond. **135**, 211 (2010)
32. A.B.P. Lever, J. Chem. Soc. **1821** (1965). doi:10.1039/jr9650001821
33. H. Miyoshi, Bull. Chem. Soc. Jpn. **47**, 561 (1974)
34. S. Stepanow, P.S. Miedema, A. Mugarza, G. Ceballos, P. Moras, J.C. Cezar, C. Carbone, F.M.F. de Groot, P. Gambardella, Phys. Rev. B **83**, 220401 (2011)
35. S. Lee, M. Yudkowsky, W.P. Halperin, M.Y. Ogawa, B.M. Hoffman, Phys. Rev. B **35**, 5003 (1987)
36. H. Senff, W. Klemm, J. Prakt. Chem. **154**, 73 (1939)
37. P.A. Reynolds, B.N. Figgis, Inorg. Chem. **30**, 2294 (1991)
38. Y. Kitaoka, T. Sakai, K. Nakamura, T. Akiyama, T. Ito, J. Appl. Phys. **113**, 17E130 (2013)
39. T. Kataoka, Y. Sakamoto, Y. Yamazaki, V.R. Singh, A. Fujimori, Y. Takeda, T. Ohkochi, S.I. Fujimori, T. Okane, Y. Saitoh, H. Yamagami, A. Tanaka, Solid State Commun. **152**, 806 (2012)
40. J.B. Goodenough, Magnetism and the chemical bond, in *Interscience Monograph on Chemistry*, ed. by F.A. Cotton (Willey, New York, 1966)
41. G. Filoti, M.D. Kuz'min, J. Bartolome, Phys. Rev. B **74**, 134420 (2006)
42. R.J. Glauber, J. Math. Phys. **4**, 294 (1963)
43. J.M. Assour, W.K. Kahn, J. Am. Chem. Soc. **87**, 207 (1965)
44. T.S. Srivasta, J.L. Przybyli, A. Nath, Inorg. Chem. **13**, 1562 (1974)
45. S. Stepanow, A. Mugarza, G. Ceballos, P. Moras, J.C. Cezar, C. Carbone, P. Gambardella, Phys. Rev. B **82**, 014405 (2010)
46. M.J. Cook, Pure Appl. Chem. **71**, 2145 (1999)
47. C.W. Miller, A. Sharoni, G. Liu, C.N. Colesniuc, B. Fruhberger, I.K. Schuller, Phys. Rev. B **72**, 104113 (2005)
48. T. Gredig, K.P. Gentry, C.N. Colesniuc, I.K. Schuller, J. Mater. Sci. **45**, 5032 (2010)
49. T. Takami, C. Carrizales, K.W. Hipps, Surf. Sci. **603**, 3201 (2009)
50. K. Manandhar, K.T. Park, S. Ma, J. Hrbek, Surf. Sci. **603**, 636 (2009)
51. A. Mugarza, R. Robles, C. Krull, R. Korytar, N. Lorente, P. Gambardella, Phys. Rev. B **85**, 155437 (2012)
52. E. Annese, J. Fujii, I. Vobornik, G. Panaccione, G. Rossi, Phys. Rev. B **84**, 174443 (2011)
53. H. Peisert, T. Schwieger, J.M. Auerhammer, M. Knupfer, M.S. Golden, J. Fink, P.R. Bressler, M. Mast, J. Appl. Phys. **90**, 466 (2001)
54. C. Monton, I. Valmianski, I.K. Schuller, Appl. Phys. Lett. **101**, 133304 (2012)
55. X. Chen, Y.S. Fu, S.H. Ji, T. Zhang, P. Cheng, X.C. Ma, X.L. Zou, W.H. Duan, J.F. Jia, Q.K. Xue, Phys. Rev. Lett. **101**, 197208 (2008)
56. M. Casarin, M. Di Marino, D. Forrer, M. Sambi, F. Sedona, E. Tondello, A. Vittadini, V. Barone, M. Pavone, J. Phys. Chem. C **114**, 2144 (2010)
57. T. Gredig, M. Werber, J.L. Guerra, E.A. Silverstein, M.P. Byrne, B.G. Cacha, J. Supercond. Nov. Magn. **25**, 2199 (2012)
58. K.A. Simonov, A.S. Vinogradov, M.M. Brzhezinskaya, A.B. Preobrajenski, A.V. Generalov, A.Y. Klyushin, Appl. Surf. Sci. **267**, 132 (2013)
59. J. Stohr, H. Konig, Phys. Rev. Lett. **75**, 3748 (1995)
60. J. Bartolome, F. Bartolome, L.M. Garcia, G. Filoti, T. Gredig, C.N. Colesniuc, I.K. Schuller, J.C. Cezar, Phys. Rev. B **81**, 195405 (2010)
61. G. Liu, T. Gredig, I.K. Schuller, Europhys. Lett. **83**, 56001 (2008)
62. K.P. Gentry, T. Gredig, I.K. Schuller, Phys. Rev. B **80**, 174118 (2009)

63. T. Gredig, C.N. Colesniuc, S.A. Crooker, I.K. Schuller, Phys. Rev. B **86**, 014409 (2012)
64. B.T. Thole, P. Carra, F. Sette, G. Vanderlaan, Phys. Rev. Lett. **68**, 1943 (1992)
65. P. Carra, B.T. Thole, M. Altarelli, X.D. Wang, Phys. Rev. Lett. **70**, 694 (1993)
66. M.D. Kuz'min, R. Hayn, V. Oison, Phys. Rev. B **79**, 024413 (2009)
67. A. König, F. Roth, R. Kraus, M. Knupfer, J. Chem. Phys. **130**, 214503 (2009)
68. K. Nakamura, Y. Kitaoka, T. Akiyama, T. Ito, M. Weinert, A.J. Freeman, Phys. Rev. B **85**, 235129 (2012)
69. T. Kroll, V.Y. Aristov, O.V. Molodtsova, Y.A. Ossipyan, D.V. Vyalikh, B. Buchner, M. Knupfer, J. Phys. Chem. A **113**, 8917 (2009)
70. X. Chen, Y.-S. Fu, S.-H. Ji, T. Zhang, P. Cheng, X.-C. Ma, X.-L. Zou, W.-H. Duan, J.-F. Jia, Q.-K. Xue, Phys. Rev. Lett. **101**, 197208 (2008)
71. Y.S. Fu, S.H. Ji, X. Chen, X.C. Ma, R. Wu, C.C. Wang, W.H. Duan, X.H. Qiu, B. Sun, P. Zhang, J.F. Jia, Q.K. Xue, Phys. Rev. Lett. **99**, 256601 (2007)
72. R. Otero, J.M. Gallego, A.L.V. de Parga, N. Martin, R. Miranda, Adv. Mater. **23**, 5148 (2011)
73. J. Kondo, Prog. Theor. Phys. **32**, 37 (1964)
74. L. Gao, W. Ji, Y.B. Hu, Z.H. Cheng, Z.T. Deng, Q. Liu, N. Jiang, X. Lin, W. Guo, S.X. Du, W.A. Hofer, X.C. Xie, H.J. Gao, Phys. Rev. Lett. **99**, 106402 (2007)
75. N. Tsukahara, S. Shiraki, S. Itou, N. Ohta, N. Takagi, M. Kawai, Phys. Rev. Lett. **106**, 187201 (2011)
76. A.D. Zhao, Q.X. Li, L. Chen, H.J. Xiang, W.H. Wang, S. Pan, B. Wang, X.D. Xiao, J.L. Yang, J.G. Hou, Q.S. Zhu, Science **309**, 1542 (2005)
77. X. Lu, K.W. Hipps, X.D. Wang, U. Mazur, J. Am. Chem. Soc. **118**, 7197 (1996)
78. N. Tsukahara, K.I. Noto, M. Ohara, S. Shiraki, N. Takagi, Y. Takata, J. Miyawaki, M. Taguchi, A. Chainani, S. Shin, M. Kawai, Phys. Rev. Lett. **102**, 167203 (2009)
79. M. Scardamaglia, G. Forte, S. Lizzit, A. Baraldi, P. Lacovig, R. Larciprete, C. Mariani, M.G. Betti, J. Nanopart. Res. **13**, 6013 (2011)
80. M. Scardamaglia, S. Lisi, S. Lizzit, A. Baraldi, R. Larciprete, C. Mariani, M.G. Betti, J. Phys. Chem. C **117**, 3019 (2012)
81. C. Iacovita, M.V. Rastei, B.W. Heinrich, T. Brumme, J. Kortus, L. Limot, J.P. Bucher, Phys. Rev. Lett. **101**, 116602 (2008)
82. J. Brede, N. Atodiresei, S. Kuck, P. Lazic, V. Caciuc, Y. Morikawa, G. Hoffmann, S. Blugel, R. Wiesendanger, Phys. Rev. Lett. **105**, 047204 (2010)
83. M.F. Crommie, Science **309**, 1501 (2005)
84. B. Stadtmuller, I. Kroger, F. Reinert, C. Kumpf, Phys. Rev. B **83**, 085416 (2011)
85. C. Isvoranu, B. Wang, E. Ataman, K. Schulte, J. Knudsen, J.N. Andersen, M.L. Bocquet, J. Schnadt, J. Chem. Phys. **134**, 114710 (2011)
86. F. Sedona, M. Di Marino, D. Forrer, A. Vittadini, M. Casarin, A. Cossaro, L. Floreano, A. Verdini, M. Sambi, Nat. Mater. **11**, 970 (2012)
87. P. Gambardella, S. Stepanow, A. Dmitriev, J. Honolka, F.M.F. de Groot, M. Lingenfelder, S. Sen Gupta, D.D. Sarma, P. Bencok, S. Stanescu, S. Clair, S. Pons, N. Lin, A.P. Seitsonen, H. Brune, J.V. Barth, K. Kern, Nat. Mater. **8**, 189 (2009)
88. C. Isvoranu, B. Wang, K. Schulte, E. Ataman, J. Knudsen, J.N. Andersen, M.L. Bocquet, J. Schnadt, J. Phys. Condens. Matter **22**, 472002 (2010)
89. C. Wäckerlin, J. Nowakowski, S.-X. Liu, M. Jaggi, D. Siewert, J. Girovsky, A. Shchyrba, T. Hählen, A. Kleibert, P.M. Oppeneer, F. Nolting, S. Decurtins, T.A. Jung, N. Ballav, Adv. Mater. **25**, 2404 (2013)
90. X. Shen, L.L. Sun, E. Benassi, Z.Y. Shen, X.Y. Zhao, S. Sanvito, S.M. Hou, J. Chem. Phys. **132**, 054703 (2010)
91. X. Shen, L.L. Sun, Z.L. Yi, E. Benassi, R.X. Zhang, Z.Y. Shen, S. Sanvito, S.M. Hou, Phys. Chem. Chem. Phys. **12**, 10805 (2010)
92. S. Schmaus, A. Bagrets, Y. Nahas, T.K. Yamada, A. Bork, M. Bowen, E. Beaurepaire, F. Evers, W. Wulfhekel, Nat. Nanotechnol. **6**, 185 (2011)
93. N. Ishikawa, M. Sugita, T. Ishikawa, S.Y. Koshihara, Y. Kaizu, J. Am. Chem. Soc. **125**, 8694 (2003)

94. N. Ishikawa, M. Sugita, N. Tanaka, T. Ishikawa, S.Y. Koshihara, Y. Kaizu, Inorg. Chem. **43**, 5498 (2004)
95. N. Ishikawa, M. Sugita, W. Wernsdorfer, Angew. Chem., Int. Ed. Engl. **44**, 2931 (2005)
96. N. Ishikawa, M. Sugita, W. Wernsdorfer, J. Am. Chem. Soc. **127**, 3650 (2005)
97. L. Margheriti, D. Chiappe, M. Mannini, P.E. Car, P. Sainctavit, M.A. Arrio, F.B. de Mongeot, J.C. Cezar, F.M. Piras, A. Magnani, E. Otero, A. Caneschi, R. Sessoli, Adv. Mater. **22**, 5488 (2010)
98. A. Lodi Rizzini, C. Krull, T. Balashov, J.J. Kavich, A. Mugarza, P.S. Miedema, P.K. Thakur, V. Sessi, S. Klyatskaya, M. Ruben, S. Stepanow, P. Gambardella, Phys. Rev. Lett. **107**, 177205 (2011)